arXiv:astro-ph/0407406v1 19 Jul 2004

High Spatial Resolution HST/NICMOS Observations of Markarian 231

F. J. Low, G. Schneider, G. Neugebauer

Steward Observatory, University of Arizona

Tucson, AZ 85721

flow@as.arizona.edu,gschneider@as.arizona.edu,gxn@as.arizona.edu

Received _____; accepted _____

Draft version:(February 2, 2008)

ABSTRACT

Observations of Markarian 231 at 1.1 μm taken with NICMOS on the Hubble Space Telescope are described. The brightness of the object in the near infrared and the inherent short-term stability of the NICMOS optical and instrumental system enables application of special observational and analysis techniques that effectively increase high spatial resolution. By these means, we set an upper limit on the size of the core of the AGN nucleus at 8 mas corresponding to a radial projected distance from the center of Markarian 231 of $\sim$ 3 pc.

Subject headings: galaxies: Seyfert infrared: galaxies, Markarian 231

1. Introduction

The ultra-luminous infrared galaxy (ULIRG; luminosity $> 10^{12}$ $L_\odot$) Markarian 231 (Mrk 231), with a bolometric luminosity of 3.3×10^{12} $L_\odot$, was first identified as a ULIRG by Rieke & Low (1972) and was found by the IRAS survey to be the most luminous object within 300 Mpc (Soifer et al. 1986). The ratio of its flux density at 25 μm ($f_\nu(25)$) to its flux density at 60 μm ($f_\nu(60)$) — $f_\nu(25)/f_\nu(60) = 0.3$ — leads to its inclusion as a "warm" IRAS galaxy (Low et al. 1988). It has the visual spectrum of a Seyfert 1 galaxy and a redshift z = 0.042 implying a projected distance scale of 800 pc asec^{-1}. From the 2MASS survey, the near infrared magnitudes within a 7″ diameter beam of Mrk 231 are J(1.25 μm) = 11.02 mag, H(1.65 μm) = 10.04 mag, and K_S(2.15 μm) = 8.94 mag (Skrutskie et al., 1997). We take the Hubble constant to be $H_0 = 75$ km s^{-1} Mpc^{-1}.

Because Mrk 231 has been considered to be a nearby infrared quasar, several observations over a range of wavelengths have been undertaken to resolve its core. Lai et al. (1998), using adaptive optics with the 3.6-m diameter CFHT Telescope, set a limit on the size of the full width at half maximum (FWHM) of the core of the active galactic nucleus (AGN) of 0.″11 (90 pc) in the near-infrared. Quillen et al. (2001) included Mrk 231 in a survey of unresolved continuum sources at 1.6 μm with the Hubble Space Telescope (HST); they set a limit on the FWHM of Mrk 231 of $\leq$ 0.″13 (100 pc). Soifer et al. (2000), using the 10-m diameter Keck Telescope, set a limit on the size of the AGN core of 0.″13 (100 pc) at 12.5 μm. Klöckner, Baan & Garrett (2003) report that the hydroxyl (mega)-maser emission shows the characteristics of a rotating, dusty, molecular torus (or thick disk) located between 30 and 100 pc from the central engine of Mrk 231. Lonsdale et al. (2003) showed, from VLBI continuum imaging observations, that at 18 cm wavelength Mrk 231 consists of a single core of FWHM $<$ 0.″005 (4 pc) plus a 0.″03 extension to the south. Further discussion of the galaxy and references emphasizing other important aspects of the

observations of Mrk 231 are given, e.g., in Lonsdale et al. and Smith et al. (1995).

The capability of using the HST at near-infrared wavelengths, its short-term (intra-orbit) optical stability (Schneider et al. 2001), and the extreme brightness of Mrk 231 offers a singular opportunity to set physically interesting limits on the size of the core in the near-infrared. In this paper we present observations of Mrk 231 made with NICMOS on the HST that were especially designed and optimized to probe the point-like source in Mrk 231.

On the basis of its far infrared color, Hines et al. (2004) include Mrk 231 as one of nine hyperluminous and "warm" ultraluminous infrared galaxies observed with NICMOS. Although the observations of Mrk 231 in Hines et al. are the same as shown here, the comparison star used by Hines et al. to define the point spread function (PSF) differs from the one used here and their reduction of the image is a preliminary one. The papers by Hines et al. and by Quillen et al. (2001) both include Mrk 231 as one of a larger sample and hence do not attach special attention to the reduction of its data. In this paper we have concentrated on the reduction of this one object and have attempted to achieve the highest spatial resolution possible with these data.

2. Observations

Observations of Mrk 231 were made in September, 1998 using the NIC1 camera and the F110M filter which has a central wavelength of 1.1 μm and filter full width at half maximum of 0.2 μm as described by Thompson et al. (1998) and in the NICMOS Instrument Handbook (Roye et al., 2003). The camera has $0\farcs043 \times 0\farcs043$ pixels corresponding to the diffraction limit of the HST at 1.0 μm, and the array has 256×256 pixels so the field of view is $\sim 11'' \times 11''$. Observations at 1.6 and 2.1 μm using the NIC2 camera accompanied the 1.1 μm observations; these and related observations will be described in Schneider &

Low (2005).

Four sequential, but separate, images of Mrk 231 were obtained. The observations were made using STEP1/NSAMP=24 multiaccum sampling (Roye et al., 2003), so the total integration time at the end of the 24-read exposure ramp for each of the individual exposures in the four point pattern was 22 seconds. After each exposure, the telescope was offset by a nominal 50.5 pixels so the active nucleus was centered on different relative positions of a pixel as well as sampling different portions of the array. In fact the observed offsets differed slightly from half integer pixels since the pixels projected onto the sky are slightly rectangular and the average offset was $\sim$ 50.6 pixels.

Four separate images of the Hubble guide star GSC 0384500748 at right ascension $12^h\ 56^m\ 15.8^s$, declination $+56^\circ\ 48^{'}\ 17\farcs7$ (J2000) — a K star — were similarly obtained in the orbit immediately after the Mrk 231 observations to determine the PSF using the same offset pattern as had been used with Mrk 231. There is no field dependency in the structure of the NIC1 camera PSF star image. The PSF star was selected primarily due to its close proximity — $\sim 4'$ — to Mrk 231 in the sky. The 2MASS survey magnitudes of the PSF star are J = 11.13 mag, H = 10.62 mag and K_S = 10.54 mag (Skrutskie et al., 1997) so it is of comparable brightness to Mrk 231 in the J band although fainter at 2.2 μm and considerably less red in its H-K color. Both sets of observations were carried out at the same spacecraft roll angle, i.e., the same field orientation, to minimize changes in differential heating to the optical telescope assembly, and better stabilize the PSF. The time and roll constraints, and the very close proximity of the PSF star in the sky, ensured the PSF was stable between the Mrk 231 and reference observations.

3. General Results and Common Reduction

The images of Mrk 231 and of the PSF star were first combined to make separate images each containing a single image of either Mrk 231 or the PSF star following the precepts outlined in Schneider & Stobie (2002). Image centroids were determined by Gaussian profile fitting after re-sampling the images onto 32 times finer grids via bi-cubic interpolation apodized by a sync function. Once the centroids were determined all images were co-aligned by shifting three of the images to the location of the fourth to the nearest integral pixel and then by interpolative sub-pixel re-sampling also by bi-cubic sinc-apodized interpolation. The four images of the PSF star, which were originally sampled according to the Nyquist criterion with $\sim$ half pixel offsets, were then median combined after registration providing super-critical sampling of the PSF star. The final image was re-sampled onto a grid of $0\farcs0054$ pixels.

The resultant image of Mrk 231 is shown as the left panel of Figure 1. The image of the PSF star is included as the right panel of Figure 1 scaled in intensity to "match" the nuclear region of Mrk 231. In the region with radius $\leq 0\farcs2$, the sum of the squares of the subtraction residuals in the difference image was minimized along with the the total energy in the difference image. The imperfectly pupil-plane masked NICMOS+HST "diffraction spikes" in the region radius $> 0\farcs2$ were simultaneously minimized. See Schneider et al. (2001) and Krist et al. (1998) for the details of HST/NICMOS target:reference PSF scaling and the effects of mis-matched PSF image structures arising from thermal de-spacing of the HST secondary mirror. The effects of temporal variability in pupil mask alignments are also discussed. Figure 2 shows median combined azimuthal radial profiles of Mrk 231 and of the PSF star and their integrated curves of growth. It is clear the nuclear region of the 1.1 μm Mrk 231 image is essentially that of an unresolved point source; the FWHM of the raw image of Mrk 231 and of the PSF star is $\sim 0\farcs10$. In both Figure 1 and Figure 2, Mrk 231

shows the presence of a host galaxy seen at low surface brightness at radius $> 0\farcs2$, but this is better examined by much deeper corongraphic imagery and will be discussed in depth by Schneider & Low (2005).

3.1. Intrinsic Core Size Limit

To recapitulate, the raw $0\farcs043 \times 0\farcs043$ pixels of NIC1 were over-sampled at 1.1 μm through the half integer pixel offset and the high signal to noise ratio available on Mrk 231 to effectively act as $0\farcs022 \times 0\farcs022$ pixels. With such well sampled images it was then possible to set a limit on the FWHM of a putative extension present in the nucleus of Mrk 231 well below the classical diffraction limit of the telescope by comparing the image structure of the Mrk 231 nucleus to that of a model made up of a core of negligible angular extent plus an assumed extension. We found that radial profiles of PSF subtracted images of various comparisons were superior in delineating the size limit of the core to direct techniques, e.g., a Richardson-Lucy deconvolution.

The left image of Figure 3 shows the result of subtracting the observed image of the PSF star, after registration and flux-scaling, from the Mrk 231 image. Images constructed by convolving the observed image of the PSF star with a model of Mrk 231 in which Mrk 231 is assumed to follow a Gaussian profile of 5.4 and 10.8 mas FWHM (middle and right) are included in Figure 3. We take the similar features seen in the middle and right hand images of Figure 3 to be a signature of the putative broadening in the model of Mrk 231.

Figure 4 shows median combined azimuthal radial profiles of the PSF subtracted images of Figure 3. The three solid curves in the figure refer to putative extensions for the core of Mrk 231, again after subtracting the observed PSF star. The FWHM parameter of

the Gaussian profile assumed for Mrk 231 is given in the figure.

In order to test the influence of noise in the image of the PSF star, the image of the observed PSF star was subtracted from a noiseless image of a model NICMOS PSF star[1], as shown by the dotted line in Figure 4. The curves for finite Gaussian extensions are virtually the same whether the image of the noiseless model PSF or observed PSF stars are subtracted. Additionally, the image of Mrk 231 itself was used in the subtraction; no significant difference in the final difference image was seen.

The negative residual which arises when normalizing the raw data to the central pixel is not surprising. This zonal under-subtraction is, in fact, replicated using either the observed PSF star (dark solid line in Figure 4) or a noiseless model PSF (dotted line in Figure 4), which suggests this residual is real and not an artifact of a mis-matched PSF. It is consistent with the amount of differential de-spacing of the HST secondary mirror expected between the Mrk 231 and PSF star observations. This residual cannot be explained by extended flux with a Gaussian radial brightness profile as it would non-physically imply that the point-source reference PSF star is wider than the core of Mrk 231.

The signature emission seen in Figure 3 is very clearly evident in Figure 4 as a non-zero emission peak at a radial distance of $\sim 0\farcs075$ — a minimum in the NICMOS diffraction pattern — in the difference image; this can be used to set a limit on the putative extent of the core of Mrk 231. It is clear from Figure 4 that a Gaussian source with a FWHM of 10 mas would be unequivocally detected in the difference image, while a Gaussian profile with a FWHM of 5 mas could be hidden in the data. We will take a FWHM of 8 mas as the limit for the putative extension of Mrk 231.

[1]http://www.stsci.edu/software/tinytim/tinytim.html

4. Discussion

4.1. Core Size

In order to place the size limit deduced from these observations in context, it is useful to consider a simple equilibrium thermal model of dust grains surrounding, and in thermal equilibrium with, a luminous hot central source. At 1.1 μm, the maximum blackbody emission (νf_ν) occurs at a temperature $\sim$3000 K. Dust grains, however, sublimate at a temperature $\sim$2000 K so a temperature of 2000 K for the dust grains will be assumed. If the central source has a bolometric luminosity 3.3×10^{12} $L_\odot$, black-body grains 0.17 pc from the central source come to equilibrium at this temperature. Silicate grains about six times further out, or 1 pc from the central source, come to equilibrium. The size limit we have deduced from these observations and NICMOS is a Gaussian FWHM of 8 mas or a projected radial distance of 3 pc at 1.1 μm. Although this is significantly smaller than previously published near-infrared limits, this does not restrict physically possible models.

We thank Paul S. Smith and Dean Hines for help with the manuscript and source selection. We also thank an anonymous referee for valuable suggestions. This work was supported, in part, by NASA grant NAG 5-3042 and 10843 to the NICMOS Instrument Definition and Guaranteed Time Observing teams. This paper is based upon observations with the NASA/ESA Hubble Space Telescope, operated by the Space Telescope Science Institute, which is operated by the Association of Universities for Research in Astronomy, Inc., under NASA contract NAS 5-26555.

REFERENCES

Hines, D. C., Low, F. J., Evans, A. S., Scoville, N. Z., & Schneider, G. 2004, in preparation

Klöckner, H-R., Baan, W. A. & Garrett, M. A. 2003, Nature, 421, 6925

Krist, John E., Golimowski, David A., Schroeder, Daniel J., & Henry, Todd J. 1998, PASP, 110, 1046

Lai, O., Rouan, D., Rigaut, F., Arsenault, R., & Gendron, E. 1998, A&A, 334, 783

Lonsdale, C. J., Lonsdale, C. J., Smith, H. E., & Diamond, P. J. 2003, ApJ, 592, 804

Low, F. J., Cutri, R. M., Huchra, J. P., & Kleinmann, S. G. 1988, ApJ, 327, L41

Quillen, A. C., et al. 2001, ApJ, 547, 129

Rieke, G. H., & Low, F. J. 1972, ApJ, 176, L95

Roye, E. & Knoll, K., et al. 2003, NICMOS Instrument Handbook, Vol. version 6.0 (Baltimore: STScI)

Schneider, G., Becklin, E. E., Smith, B. A., Weinberger, A. J., Silverstone, M., & Hines, D. 2001, AJ, 121, 525

Schneider, G. & Low, F. J. (2005) in preparation

Schneider, G., & Stobie, E. 2002. in Astronomical Data Analysis Software and Systems XI, Pushing the Envelope: Unleashing the Potential of High Contrast Imaging with HST, eds. D. A. Bohlender, D. Durand, & T. H. Handley (San Francisco: Astronomical Society of the Pacific), 382

Skrutskie, M. F., et al. 1997. in The Impact of Large Scale Near-IR Sky Surveys, The Two Micron All Sky Survey (2MASS): Overview and Status., eds. F. Garzon, & e. al. (Dordrecht: Kluwer Academic Publishing Company), 25

Smith, Paul S., Schmidt, Gary D., Allen, Richard G., & Angel, J. R. P. 1995, ApJ, 444, 146

Soifer, B. T., et al. 2000, AJ, 119, 509

—. 1986, ApJ, 303, L41

Thompson, R., Rieke, M., Schneider, G., Hines, D., & Corbin, M. 1998, ApJ, 492, L95

This manuscript was prepared with the AAS LaTeX macros v5.2.

Fig. 1.— NICMOS Camera NIC1 F110M images are given of Mrk 231 (left) and of the PSF reference star GSC 0384500748 (right) with the flux density renormalized as discussed in the text. Both images are 7.″5 × 7.″5 and have been constructed from four-point half-integral pixel stepped observations, as described in the text, providing effective spatial sampling of 0.″022 per re-sampled pixel. Images are shown with a logarithmic stretch of [-2] to [+1] dex ADU $\sec^{-1}$ pixel^{-1}. The diffuse brightening in the circumnuclear region beyond the display-saturated first Airy ring in Mrk 231 compared to GSC 0384500748 is due to the presence of the host galaxy and is discussed in Schneider & Low (2005).

Fig. 2.— The azimuthally median filtered surface brightness radial profiles (top) and the integrated flux densities in appropriate annuli (bottom) of Mrk 231 and the reference PSF star are shown. The PSF star has been scaled as described in the text and in Schneider et al. (2001) and Krist et al. (1998). It is seen that the nuclear cores of the two objects are extremely well matched at radii $r < 0.''2$. At $r > 0.''2$ the contribution to the surface brightness due to the host galaxy is readily apparent (also see Figure 1).

Fig. 3.— Images of Mrk 231 are shown after subtracting the flux-scaled and concentricity registered reference PSF star image as discussed in text – left: Mrk 231 as observed– middle: Mrk 231 assumed to follow a 5.4 mas FWHM Gaussian profile – right: Mrk 231 taken to have a 10.8 mas FWHM Gaussian profile. Images are stretched from -2% (black) to +7% (white) of the un-subtracted peak intensity of the Mrk 231 nucleus. Images are 0.″460 × 0.″460.

Fig. 4.— Radial brightness profiles (azimuthal median of all pixels in a 5.4 mas wide annuli) of the PSF subtracted Mrk 231 images shown in Figure 3 are given. As discussed in the text, the solid lines refer to the FWHM of Gaussian profiles assumed for the core of Mrk 231. The curve marked "0 mas" represents the image of the observed PSF star. The subtraction of a noiseless high fidelity model PSF, rather than the image of the observed PSF star, from

the observed Mrk 231 image is shown by the dotted line. Error bars represent standard deviations (1-σ) of all pixels in each annulus about the median value in each annulus.

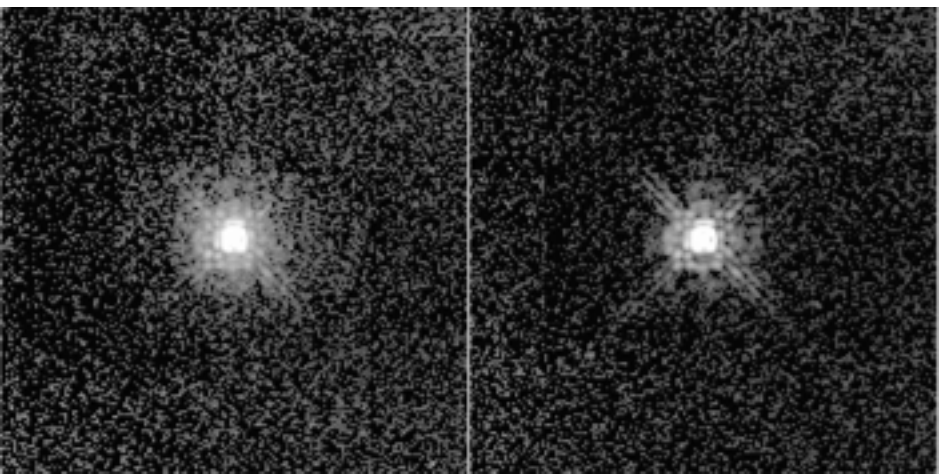

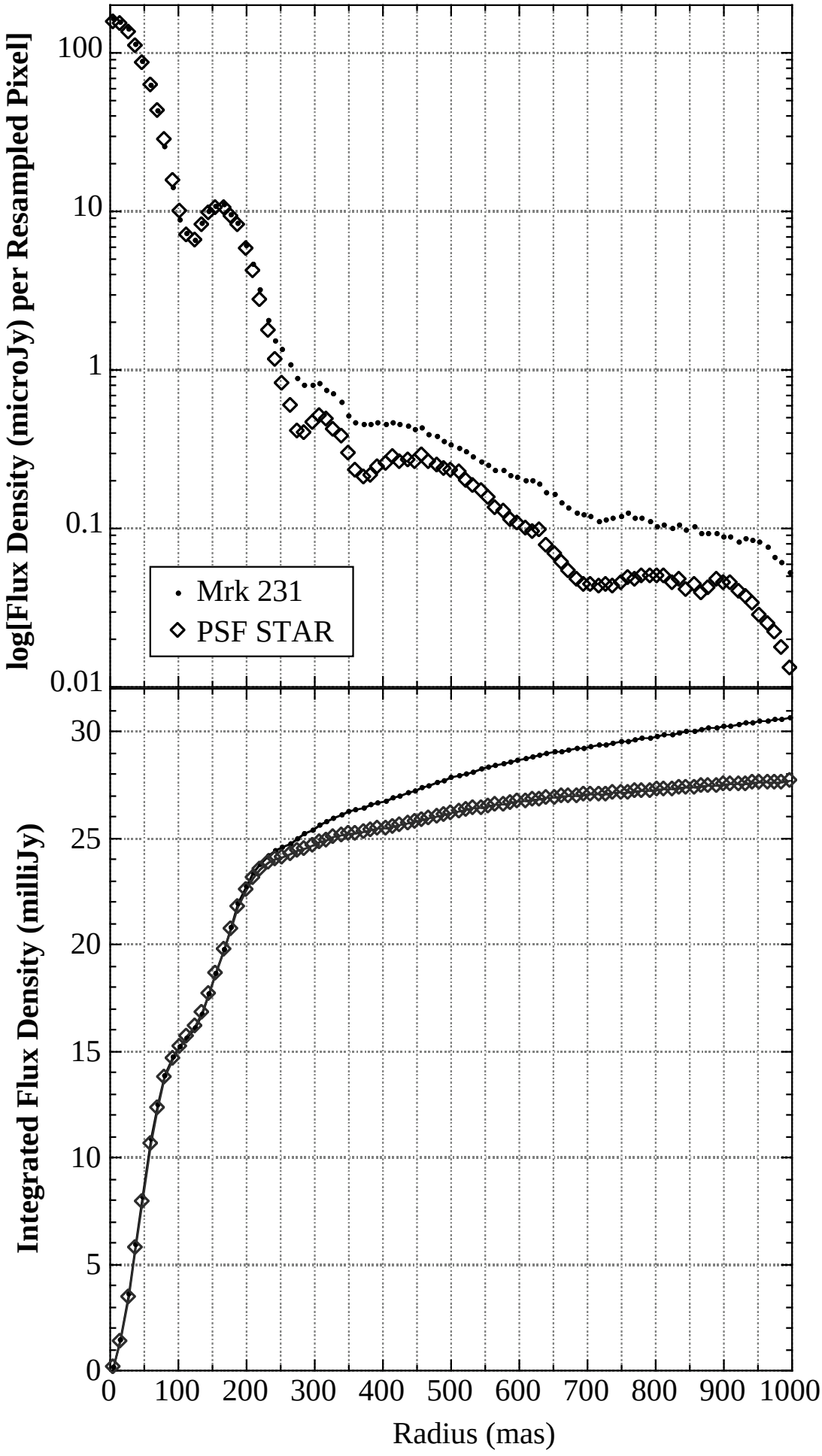
log[Flux Density (microJy) per Resampled Pixel]
100
10
1
0.1
0.01
Mrk 231
PSF STAR
Integrated Flux Density (milliJy)
30
25
20
15
10
5
0
0
100
200
300
400
500
600
700
800
900
1000
Radius (mas)

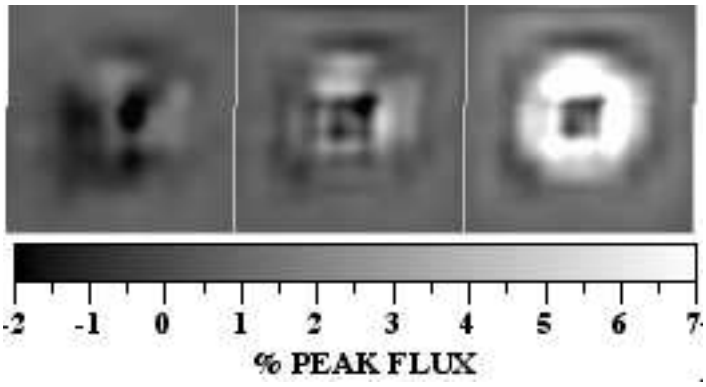
-2
-1
0
1
2
3
4
5
6
% PEAK FLUX

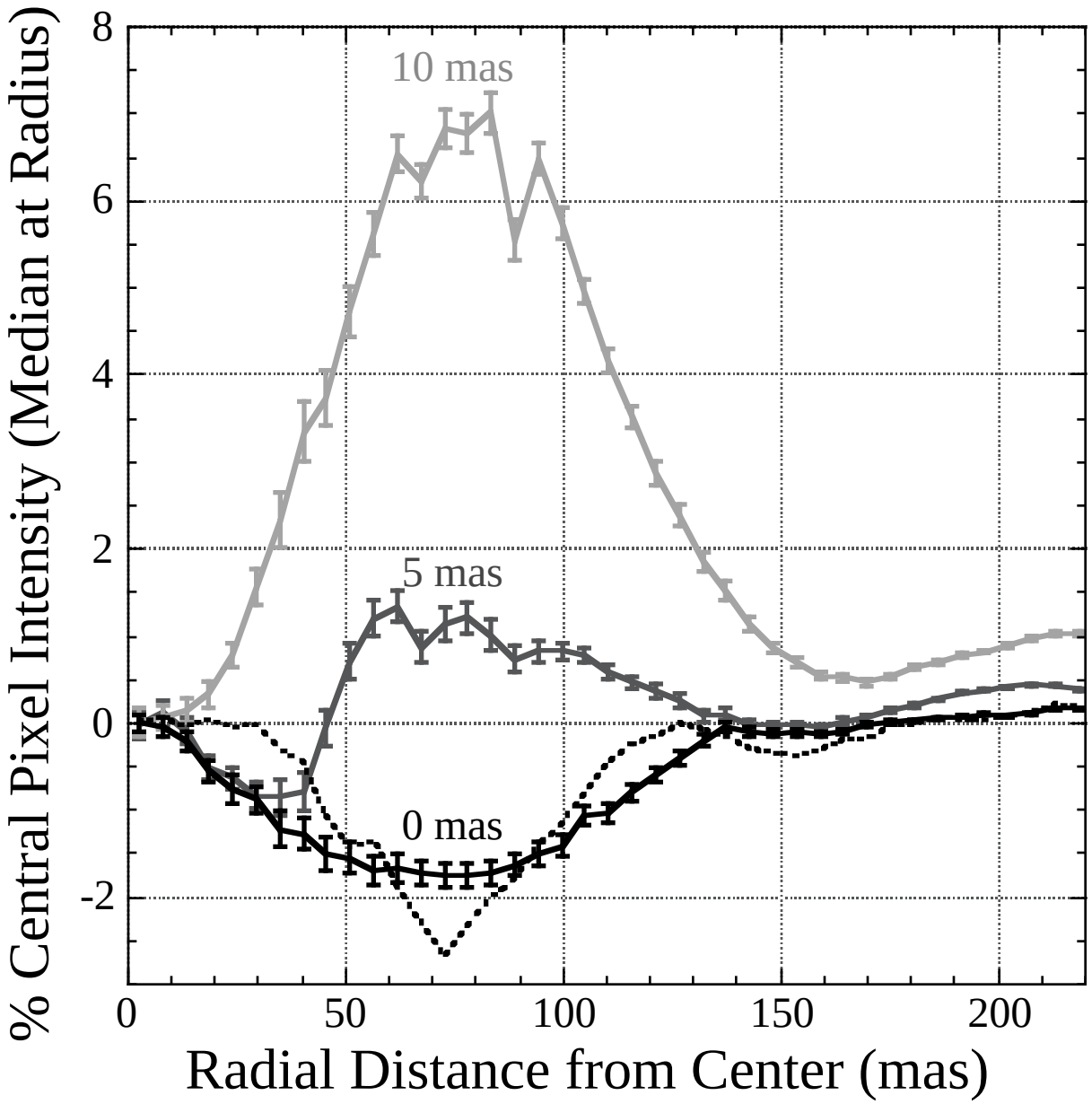
% Central Pixel Intensity (Median at Radius)
8
6
4
2
0
-2
10 mas
5 mas
0 mas
0
50
100
150
200
Radial Distance from Center (mas)